Effects of nanomorphological changes on the performance of solar cells with blends of poly[9,9'-dioctyl-fluorene-co-bithiophene] and a soluble fullerene



2009 Nanotechnology 20 025202

(http://iopscience.iop.org/0957-4484/20/2/025202)

Nanotechnology **20** (2009) 025202 (9pp) doi:10.1088/0957-4484/20/2/025202

# Effects of nanomorphological changes on the performance of solar cells with blends of poly[9,9′-dioctyl-fluorene-co-bithiophene] and a soluble fullerene

**Jen-Hsien Huang[1], Zhong-Yo Ho[2], Dhananjay Kekuda[3], Yung Chang[4,5], Chih-Wei Chu[3,6,7] and Kuo-Chuan Ho[1,2,7]**

[1] Department of Chemical Engineering, National Taiwan University, Taipei 10617, Taiwan
[2] Institute of Polymer Science and Engineering, National Taiwan University, Taipei 10617, Taiwan
[3] Research Center for Applied Sciences, Academia Sinica, Taipei, 11529, Taiwan
[4] R & D center for Membrane Technology, Chung Yuan Christian University, Taoyuan 320, Taiwan
[5] Department of Chemical Engineering, Chung Yuan Christian University, Taoyuan 320, Taiwan
[6] Department of Photonics National Chiao Tung University, Hsinchu 300, Taiwan

E-mail: kcho@ntu.edu.tw and gchu@gate.sinica.edu.tw

Received 16 September 2008, in final form 22 October 2008
Published 9 December 2008
Online at stacks.iop.org/Nano/20/025202

**Abstract**

Controlled nanophase segregation within the blended films of a conjugated polymer and a soluble fullerene has enabled us to form a continuous transfer pathway for the carriers, thereby increasing the photocurrent generation for polymer photovoltaic devices. Here, we study the effects of nanomorphological changes on the performance of polymer solar cells using blended films of poly[9, 9′-dioctyl-fluorene-co-bithiophene] (F8T2) and [6,6]-phenyl-C61-butyric acid methyl ester (PCBM). Different weight ratios of the F8T2 and PCBM blends in various solvents were studied at different annealing temperatures. The morphology of the films seems to be a strong function of the processing conditions. The power conversion efficiency (PCE) of the photovoltaic devices has improved significantly from 0.34% to 2.14% under air mass 1.5 simulated solar illumination (100 mW $cm^{-2}$), which could be attributed to the nanomorphological changes in the films.

(Some figures in this article are in colour only in the electronic version)

## 1. Introduction

Over the last decade, the technological developments for renewable energies have become increasing important in order to meet the world's rising demand for energy and environmental issues. Among all the different kinds of renewable energies, solar energy appears to be the most attractive because of its truly clean and inexhaustible nature. Photovoltaic (PV) devices based on organic materials, both small molecules and conjugated polymers, have attracted much attention recently due to their potential production advantages [1–3]. In addition, polymer PV cells also offer the ability to tailor the chemical structure of polymers to achieve better opto-electronic characteristics. Among the various schemes of device structure, bulk heterojunction (BHJ) has been the most widely employed for polymer solar cells. The interpenetrating network of blended electron donor and acceptor materials provides a large interface between the two materials, allowing significant exciton separation and carrier transport to the respective electrodes. However, the power

[7] Authors to whom any correspondence should be addressed.

 

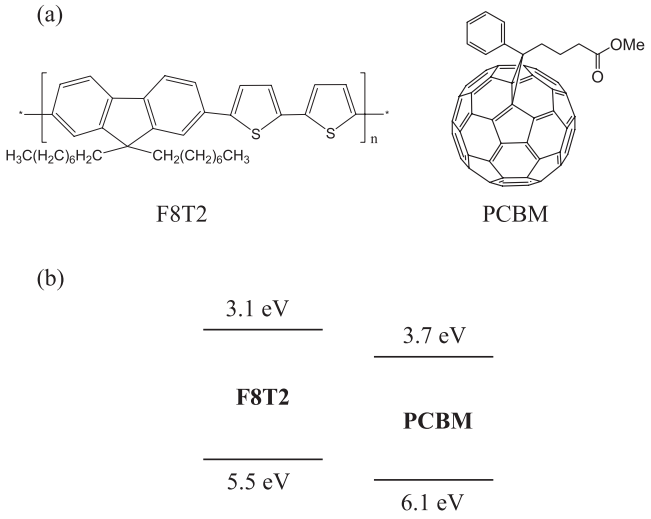


**Figure 1.** (a) Chemical structure of F8T2 and PCBM and (b) energy-level diagrams of the F8T2:PCBM mixed film.

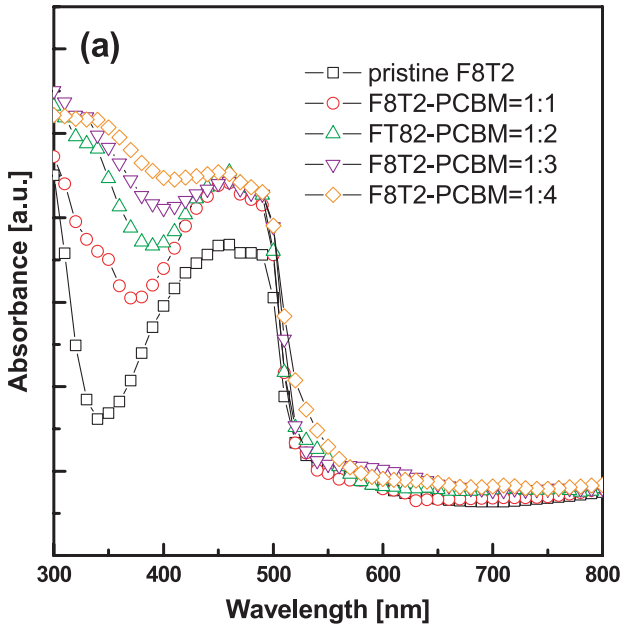


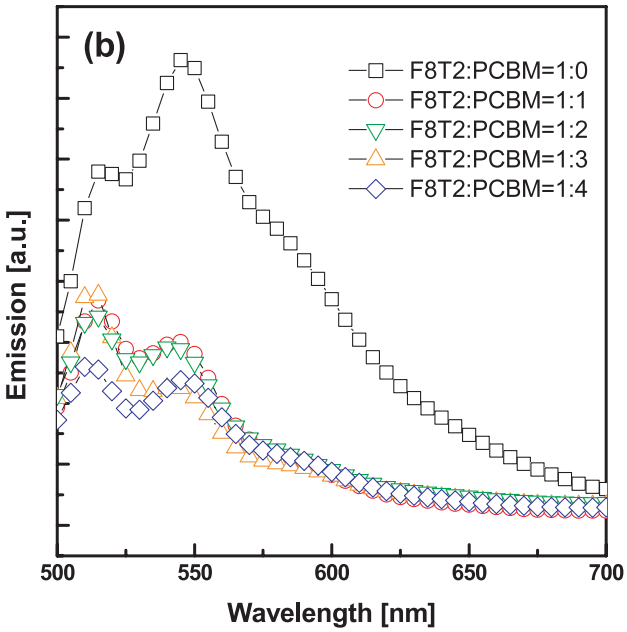


**Figure 2.** UV–vis absorption and photoluminescence spectra of F8T2:PCBM films with various blending ratios.

conversion efficiency (PCE) is still limited by the space–charge effects due to the imbalance of electron ($\mu_e$) and hole mobility ($\mu_h$). In general, hole transport is less efficient than electron transport, and the increase in hole mobility can balance the charge transport. Several methods have been proposed to solve the mismatch of the charge mobilities, these include solvent and thermal annealing [4–7], increasing the interface for charge separation [8], and varying the molar ratio between the donor and acceptor [9, 10].

Recently, fluorene based copolymers have demonstrated promising semiconductor materials for polymer PVs. Polyfluorene copolymers are well known for their high charge carrier mobility, good processability, and high absorption coefficients. The physical properties of polyfluorene derivatives can be controlled by designing various copolymers. Currently, PCEs approaching 3.5%–5.5% have been reported by several groups employing devices based on blended films of polyfluorene copolymers and PCBM [11–14]. Among this class of polymers, poly[9,9′-dioctyl-fluorene-co-bithiophene] (F8T2) has excellent properties in both the hole transporting regime [15–19] and thermotropic liquid crystallinity to allow better packing of the polymer via self-assembly [20]. Based on these properties, a more balanced charge transport can be expected in systems using F8T2:PCBM and are demonstrated in this paper. Moreover, in this paper, we report the effect of nanomorphological changes on the photovoltaic performance based on a F8T2:PCBM BHJ system.

## 2. Experimental details

### *2.1. Fabrication of PV devices*

The polymer PV cells in this study consist of a F8T2:PCBM blended thin film sandwiched between a transparent indium tin oxide (ITO) anode and a metal cathode. Prior to device fabrication, the ITO-coated glass substrates (1.5 × 1.5 $cm^2$) were ultrasonically cleaned in detergent, de-ionized water, acetone, and isopropyl alcohol. Afterwards, the substrates were treated with UV ozone for 15 minutes, and a layer of poly(ethylene dioxythiophene): polystyrenesulfonate (PEDOT:PSS, ∼30 nm) was subsequently spin-coated on to the substrate. After baking at 130 °C for one hour, the substrates were transferred to a nitrogen-filled glove box. The polymer PV devices were fabricated by spin-coating a blended solution of F8T2:PCBM on to the PEDOT:PSS modified substrate at 600 rpm for 60 seconds, and placed in a covered glass petri dish. Subsequently, the films were annealed on a hotplate at various temperatures for 20 minutes. The blended solution was prepared by dissolving both F8T2 and PCBM in DCB in a 1:1 weight ratio, followed by continuous stirring for 12 hours at 50 °C. Finally, 30 nm calcium and 100 nm aluminum

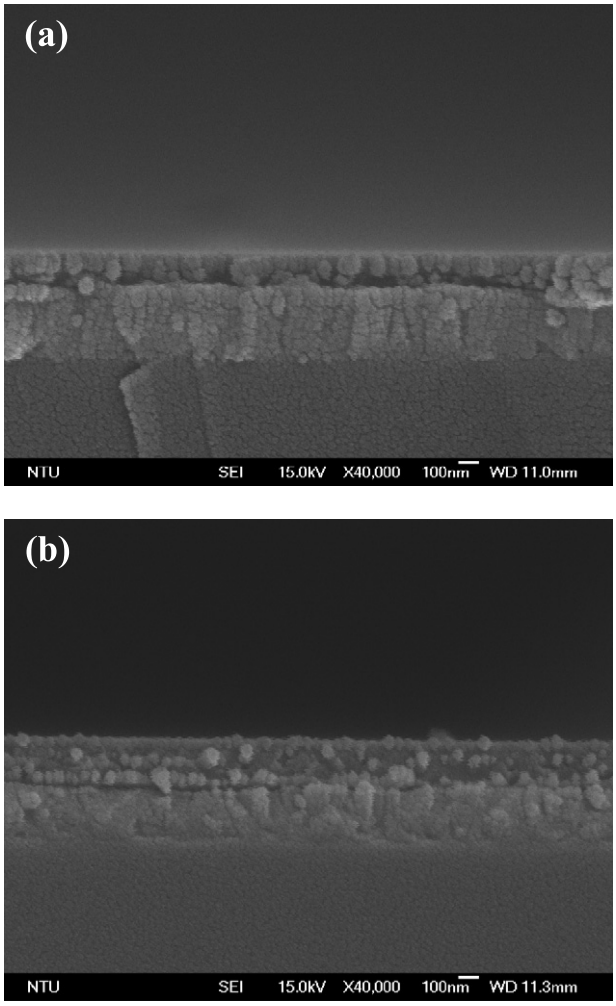


**Figure 3.** SEM side views of F8T2:PCBM blend films cast from DCB with PCBM in (a) 50 wt% and (b) 80 wt%.

layers were thermally evaporated thorough a shadow mask at a pressure below $6 \times 10^{-6}$ Torr. The active area of the device was 0.12 $cm^2$.

### 2.2. *Fabrication of hole- and electron-only devices*

In the hole-only devices, Ca was replaced with $MoO_3$ ($\Phi$ = 5.3 eV), which has been shown to provide a good hole injection contact in F8T2:PCBM systems [21]. The $MoO_3$ was thermally evaporated to a thickness of 20 nm and then capped with 50 nm of Al. For the electron-only devices, the PEDOT:PSS layer was replaced with $CsCO_3$ ($\Phi$ = 2.9 eV), which has been used as an efficient electron injection layer [22]. The $Cs_2CO_3$ was thermally evaporated with a thickness of approximately 2 nm. For both hole-only and electron-only devices, annealing of the active layer was performed at 130 °C for 20 minutes.

### 2.3. *Characterization of polymer films*

Current–voltage ($I$–$V$) characteristics were measured in the glove box under a nitrogen atmosphere. The photovoltaic

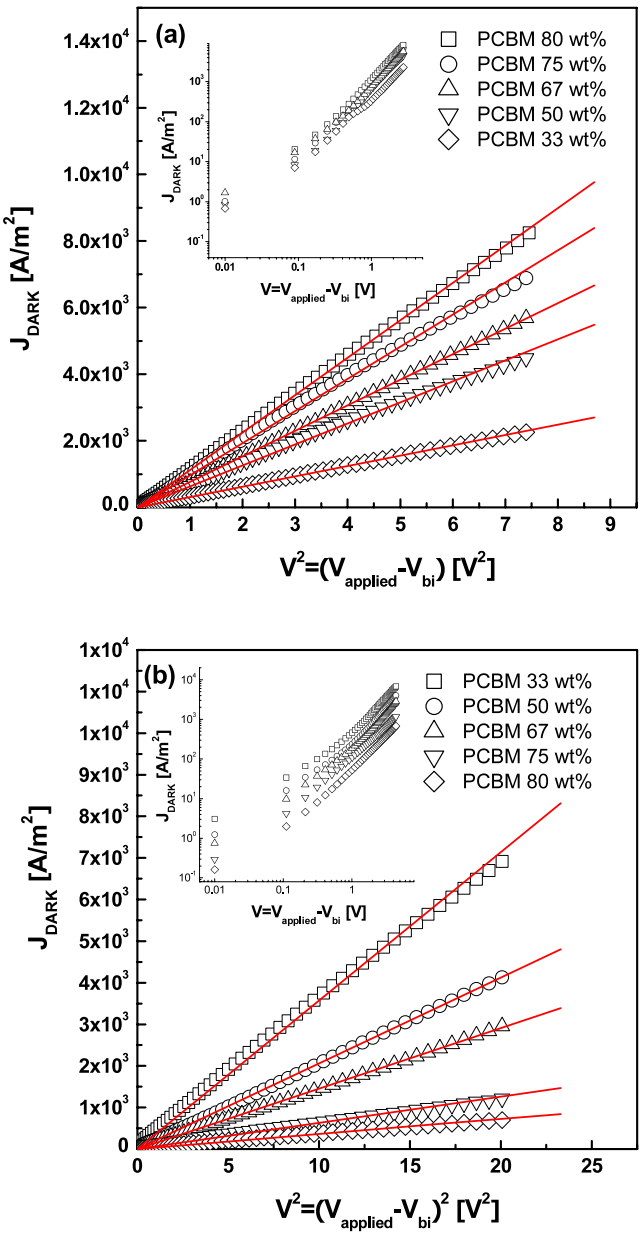


**Figure 4.** The calculated charge mobility as a function of PCBM concentration for (a) electron-only and (b) hole-only PV devices. The solid lines show the fit to experimental data using the SCLC model.

performance was characterized with a solar simulator (Thermal Oriel 1000 W) with simulated AM 1.5 G irradiation at 100 mW $cm^{-2}$. The light intensity was calibrated by a mono-silicon photodiode with KG-5 color filter (Hamamatsu, Inc.). For measuring the absorption and photoluminescence (PL) emission properties of polymer films, samples were fabricated via spin-coating on a glass substrate. The UV–vis absorption spectra were measured using a Jasco-V-670 UV–visible spectrophotometer. PL spectra were obtained using a Hitachi F-4500 photoluminescence spectrophotometer. Cross sections of the thin films were observed using a scanning electron microscopy (SEM, Hitachi S-4700). Surface morphologies were imaged using an atomic force microscope (AFM, Digital instrument NS 3a controller with D3100 stage).

**Table 1.** A summary of the charge mobility and the cell performance of parameters, indicating $J_{SC}$, $V_{OC}$, FF and PCE as functions of PCBM concentration.

| Sample | $\mu_e$ ($m^2\ V^{-1}\ s^{-1}$) | $\mu_h$ ($m^2\ V^{-1}\ s^{-1}$) | $\mu_e/\mu_h$ | $J_{SC}$ (mA $cm^{-2}$) | $V_{OC}$ (V) | FF (%) | PCE (%) |
|---|---|---|---|---|---|---|---|
| PCBM 33 wt% | $5.89 \times 10^{-8}$ | $1.46 \times 10^{-7}$ | 0.40 | 1.96 | 0.90 | 47.3 | 0.85 |
| PCBM 50 wt% | $1.11 \times 10^{-7}$ | $8.24 \times 10^{-8}$ | 1.35 | 2.92 | 0.91 | 47.1 | 1.23 |
| PCBM 67 wt% | $1.44 \times 10^{-7}$ | $6.20 \times 10^{-8}$ | 2.32 | 2.78 | 0.88 | 46.3 | 1.16 |
| PCBM 75 wt% | $1.80 \times 10^{-7}$ | $2.44 \times 10^{-8}$ | 7.37 | 2.46 | 0.88 | 42.4 | 0.95 |
| PCBM 80 wt% | $1.90 \times 10^{-7}$ | $1.42 \times 10^{-8}$ | 13.38 | 1.04 | 0.78 | 41.3 | 0.34 |

The thicknesses of all polymer films were measured using a surface profiler (Alpha-step IQ, KLA Tencor). XPS spectra were recorded on a PHI 5000 VersaProbe (ULVAC-PHI, Chigasaki, Japan) system using a microfocused (100 $\mu$m, 25 W) Al x-ray beam A Wienfiltered $C_{60}^+$ ion source (IOG C60-10, Ionoptika, Chandler's Ford, UK) was operated at 10 nA and 10 kV. The angle between the $Ar^+$ and $C_{60}^+$ ion beam was 33°. The ion-beam current was measured with the target current of an Au foil. The base pressure of the main chamber ($<1 \times 10^{-7}$ Pa) was achieved by evacuation using turbomolecular and ion-getter pumps.

## 3. Results and discussions

### *3.1. The effect of PCBM blending ratios*

Figure 1 shows the chemical structures of F8T2 and PCBM and their energy levels. It can be seen that the offset between the lowest unoccupied molecular orbital (LUMO) levels of donor and acceptor is sufficient for charge separation. The PCBM loading in the blend system is an important parameter in controlling the performance of the polymer solar cells. Figures 2(a) and (b) show the UV–vis absorption and PL emission spectra, respectively, of the pristine F8T2 blended with various molar ratios of PCBM. It can be seen that the pristine F8T2, with maximum absorption at 460 nm, only absorbs light at wavelengths less than 500 nm due to its wide energy band gap (2.4 eV). As an active layer in the solar cell, it depresses the extraction of the photocurrent for absorption within a narrow range. Although the absorption between 300 and 500 nm of F8T2 can be enhanced by blending with PCBM as shown in figure 1(a), the spectral coverage is still very poor. However, a large open circuit voltage ($V_{OC}$) can be expected due to the large difference between the HOMO of F8T2 and LUMO of PCBM [19]. Figure 2(b) shows PL spectra for the same set of films as shown in figure 2(a). The F8T2 shows an emission maximum at 545 nm with a vibronic feature at 515 and 585 nm. A significant quenching in PL is observed when F8T2 is blended with PCBM. The highest quenching, by a factor of about 2.67, was achieved with the 50 wt% PCBM, and no further quenching can be achieved with larger PCBM loadings. These results provide evidence for exciton dissociation, and thus efficient solar cells.

SEM was employed to gain insight on the nanoscale features within the F8T2:PCBM film cast from 1,2-dichlorobenzene (DCB). Based on the cross-sectional SEM images shown in figures 3(a) and (b), the film thicknesses are approximately 170–200 nm with nanospheres embedded in the blended films. These nanospheres contribute to the fact that polymer F8T2 adopts a coiled conformation. Hence, the nanospheres become smaller and less numerous with decreasing F8T2 concentrations (figures 3(a) and (b)). The results are similar to those of the the blended films based on poly[2-methoxy-5-(3,7-dimethyloctyloxy)]-1,4-phenylenevinylene (MDMO-PPV) and PCBM systems [23–25]. As the polymer concentration is reduced to 20 wt%, the spherical polymer density is insufficient to achieve complete percolation for charge transport across the film. Hence it is expected that some of the photoexcitations will lead to an increase in charge recombination.

To further explore the dependence of charge transfer properties on nanomorphologies introduced by varying the PCBM loading in the blend, we have performed dark current measurements on hole-only and electron-only devices. The electron and hole mobilities can be determined precisely by fitting the plot of the dark current versus the voltage ($J$–$V$) curves for single carrier devices to the SCLC model [26, 27]. The dark current is given by $J = 9\varepsilon_0\varepsilon_r\mu V^2/8L^3$ [28], where $\varepsilon_0\varepsilon_r$ is the permittivity of the polymer, $\mu$ is the carrier mobility, $L$ is the device thickness. From the capacitance–voltage measurements, we have obtained a relative dielectric constant $\varepsilon_r$ of 2.5 for F8T2. Figure 4 shows the dark current densities of F8T2:PCBM blends with different ratios in both electron-only and hole-only devices. As in figure 4, the solid lines show the fits to the data using the SCLC model, and the insert shows the log $J$–log $V$ curves. The applied voltage has been corrected for the built-in voltage ($V_{bi}$), which arises from the difference in the work function of the contacts, so that $V = V_{applied} - V_{bi}$. $V_{bi}$ values are 0.1 V for both electron-only and hole-only devices. The calculated mobility of electrons and holes in F8T2:PCBM BHJ devices are presented as a function of blending ratios in table 1. These devices were all annealed at 130 °C before the deposition of the aluminum electrode. A gradual increase of $\mu_e$ with increasing PCBM concentration can be observed from 33 to 80 wt%. The $\mu_e$ with 80 wt% PCBM is $2.1 \times 10^{-7}\ m^2\ V^{-1}\ s^{-1}$, which is very close to that of pristine PCBM ($1.9 \times 10^{-7}\ m^2\ V^{-1}\ s^{-1}$) [29]. This indicates that the electron transport has approached a saturated condition. However, the $\mu_h$ decreases with increasing PCBM concentrations. For the film containing 50 wt% PCBM, electron and hole mobilities of $\mu_e = 1.11 \times 10^{-7}\ m^2\ V^{-1}\ s^{-1}$ and $\mu_h = 8.24 \times 10^{-8}\ m^2\ V^{-1}\ s^{-1}$, respectively, were observed, which is the most balanced charge transport ($\mu_e/\mu_h = 1.35$) obtained in this study.

Table 1 also shows the photovoltaic characteristics as a function of PCBM molar ratios. A maximum value of $J_{SC}$, and

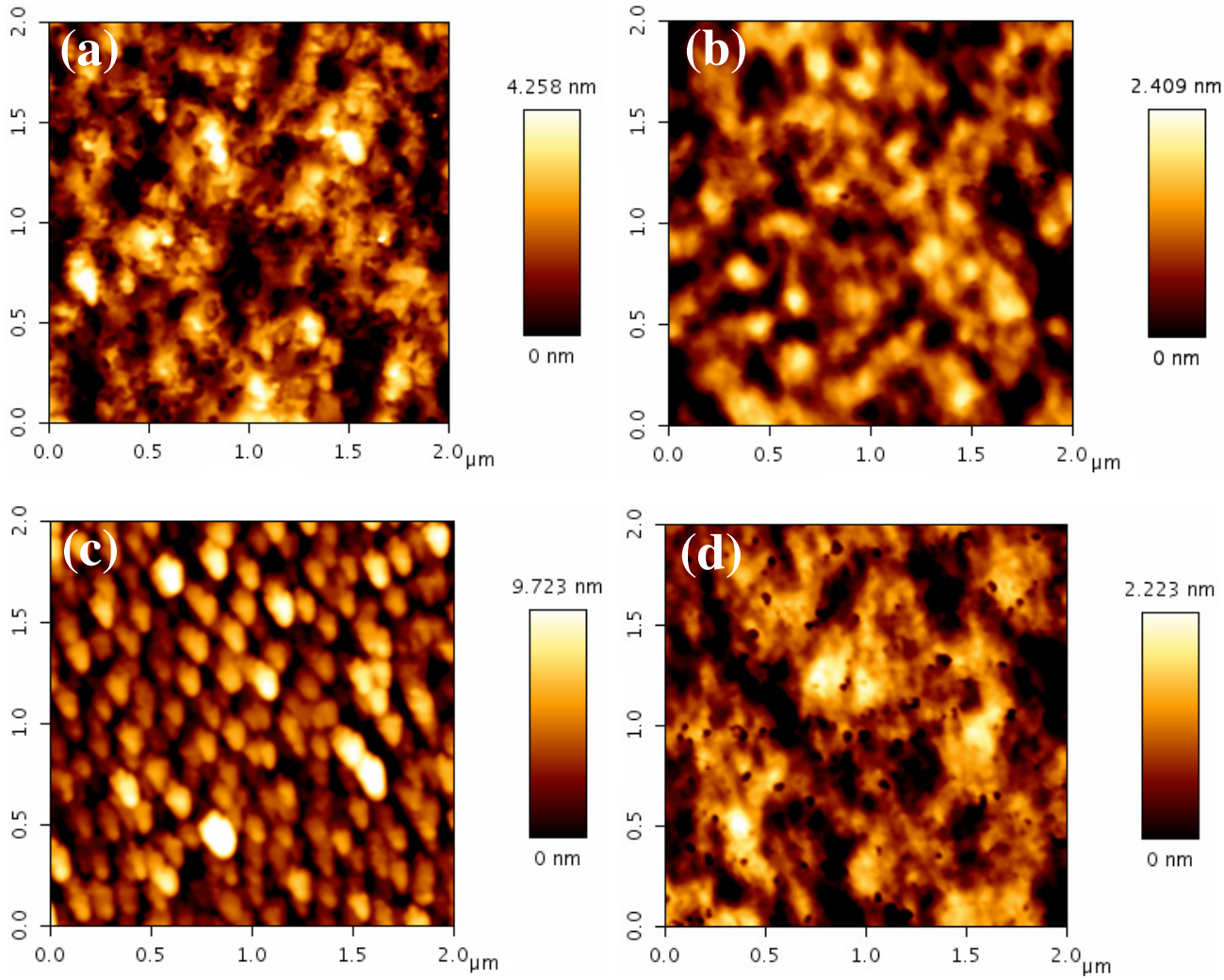


**Figure 5.** AFM images of the blended films cast from (a) TCB, (b) DCB, (c) TE, and (d) CF.

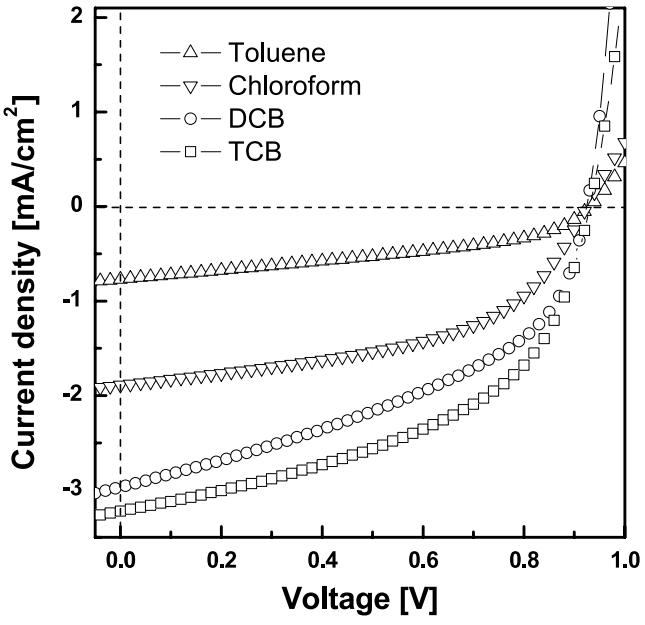


**Figure 6.** $J$–$V$ curves under illumination of F8T2:PCBM cast from different solvents.

PCE can be observed for the PV device with 50 wt% of PCBM. Both $J_{SC}$, and PCE decrease with PCBM loading larger than 50 wt%. This can be most probably attributed to an increased aggregation of the PCBM, which influences the separation of charges, as shown in figure 3. Furthermore, an unbalanced charge transport was established due to the large fullerene ratio. Hence, both the $J_{SC}$ and PCE decrease with larger fullerene molar ratios because of the two reasons described above. In addition, the values for $V_{OC}$ and FF vary monotonically when the PCBM content in the blended films is increased. This can be rationalized by the incomplete charge generation and transport resulting from the aggregation of PCBM. The best performance was obtained with an active layer thickness of approximately 200 nm, containing 50 wt% of the PCBM, which demonstrated a $J_{SC}$ of 2.92 mA cm$^{-2}$, $V_{OC}$ of 0.93 V, FF of 47.1%, and PCE of 1.23%.

### *3.2. The solvent effects*

In order to investigate the effects of different solvents on the morphology and the performance of solar cells based on F8T2:PCBM, several solvents with different evaporation rates

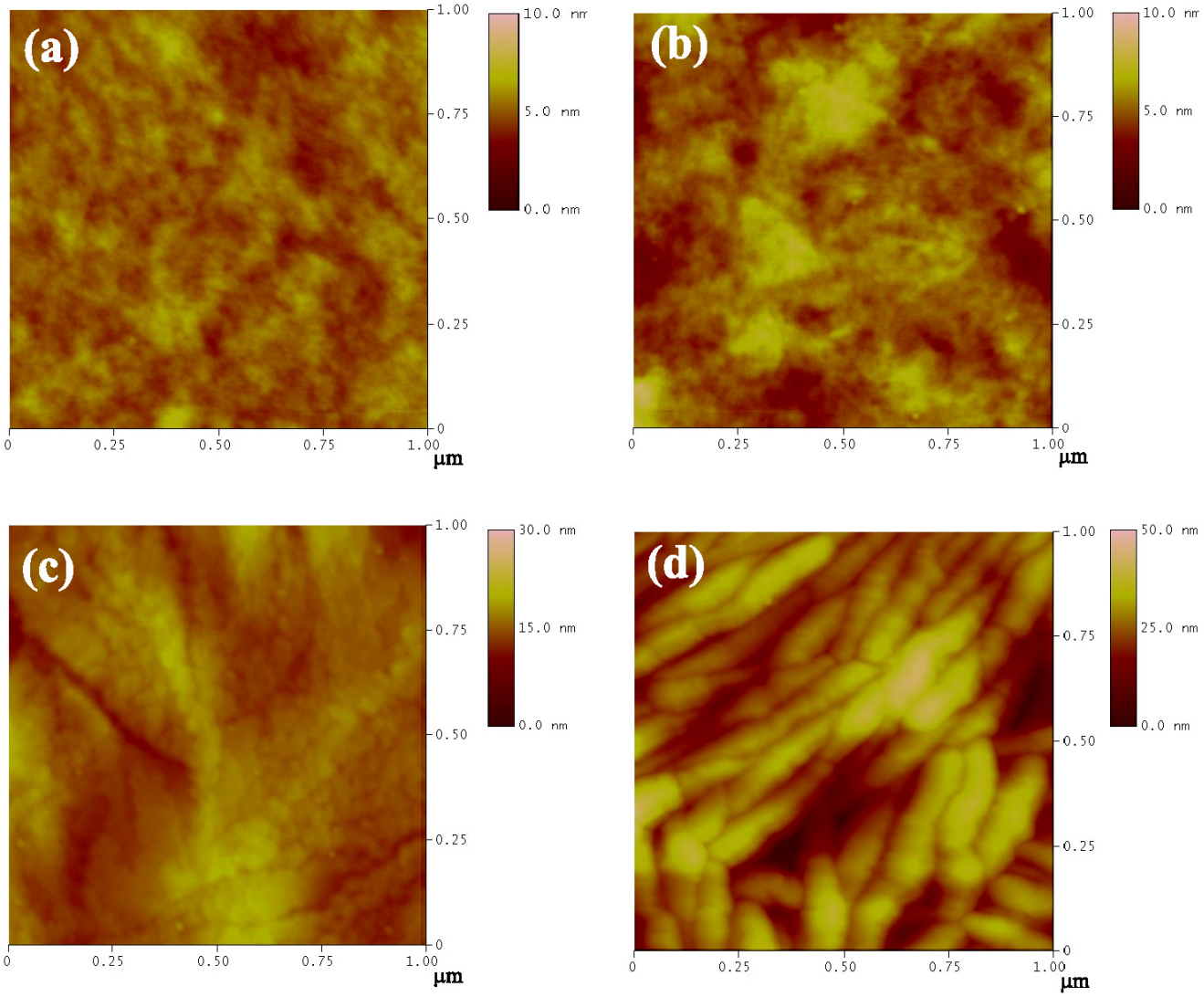


**Figure 7.** AFM images of the blended films at various annealing temperatures (a) as-cast film, (b) 130 °C, (C) 190 °C, and (d) 250 °C.

were investigated, including 1,2,4-trichlorobenzene (TCB), 2,4-dichlorobenzene (DCB), toluene (TE), and chloroform (CF), which have the corresponding boiling points of 218 °C, 180 °C, 110 °C, and 60 °C, respectively. All samples were fabricated via the slow growth method and annealed at 130 °C. The AFM topographies of F8T2:PCBM spin-coated from TCB, DCB, CF, and TE are shown in figure 5. The blend ratio was chosen to be 1:1 by weight. The images were obtained in tapping mode for a $2 \times 2$ $\mu m^2$ surface area. The phase images of the films spin-coated from TCB and DCB show coarse chainlike features across the surfaces. The features are assigned to the domains of pristine F8T2 crystallites originating from the highly tight stack of several polymer chains. This feature has been previously observed in P3HT:PCBM blends using the slow growth method with high boiling point solvents such as TCB or DCB. In the slow growth approach, the film is kept in the liquid phase after spin-coating by using a high boiling point solvent. However, the film that was spin-coated from TCB reveals a rather uneven surface (root mean square roughness (RMS) of 3.6 nm) compared to the one obtained from DCB (RMS of 2.2 nm). The rougher active surface layer can provide a large metal–polymer interface, which is more suited to efficient charge collection. On the other hand, low boiling point solvents such as CF suppress the formation of F8T2 crystallites, with the resulting film consisting of mixed domains due to the fast growth rate. In the case of the film that was spin-coated from TE, it has a distintive morphology when compared to that fabricated from TCB, DCB and CF. A more pronounced phase segregation with a domain size of 100–150 nm is observed. Furthermore the TE film also exhibits much greater height variations on its surface. Since the solubility of PCBM in toluene is lower than in the other solvents, we believe those domains mainly consist of PCBM, and they disconnect the charge transport channel from F8T2, resulting in a poor interface for exciton dissociation.

The $J$–$V$ curves under illumination for the four devices fabricated from different solvents (TCB, DCB, CF and TE) are shown in figure 6. The active layers are spin-coated from F8T2:PCBM in 1:1 ratio by weight and annealed at 130 °C. The $J_{SC}$ values of the devices fabricated from TCB, DCB, CF

and TE are 3.22, 2.96, 1.89, and 0.77 mA $cm^{-2}$, respectively, and the FF values are 48.8, 43.5, 50.2, and 40.6%, respectively. The $V_{OC}$ values are approximately 0.93 V for all devices. The highest PCE value, 1.46%, and the highest and $J_{SC}$ were obtained using TCB solvent. This can be rationalized by the fact that the slow growth method allows self-organization to take place and a charge transport channel can be formed, leading to a higher photocurrent. It has been demonstrated that the slow growth approach can not only favorably enhance morphology, but also increase the $\mu_h$ of polymer [30], leading to a more balanced charge transport. In this system, hole transport is slower than electron transport. Therefore, the increase in hole mobility is a positive effect in terms of solar cell efficiency. For the F8T2:PCBM blend fabricated from TCB, the hole and electron mobilities are $9.33 \times 10^{-8}$ and $1.21 \times 10^{-7}$ $m^2$ $V^{-1}$ $s^{-1}$, respectively, leading to a more balanced charge transport ($\mu_e/\mu_h = 1.29$) when compared to the device fabricated using DCB as solvent. However, the serious phase separation in the cases of CF and TE suppresses the exciton separation and dramatically reduces the photocurrent collection.

### *3.3. The annealing effects*

The AFM images of F8T2:PCBM (1:1) annealed at different temperatures are shown in figure 7. For the as-cast film, the surface is very smooth with a RMS roughness of 0.55 nm. However, after undergoing thermal treatment at 130, 190, and 250 °C for 20 minutes, the RMS roughness becomes 0.91, 1.98, and 6.73 nm. Moreover, lamella-like crystallites can be easily observed from the film annealed at 250 °C. The crystallization is assigned to the domains of F8T2 crystallites originating from the highly tight stack of several polymer chains. It has been previously reported that the polymer crystallites formed during thermal annealing can enhance the $\mu_h$ significantly [31].

The cross-sectional SEM images (figure 8), also provide insight on the nature of the F8T2:PCBM interface. Based on the SEM images, the F8T2 nanospheres were well dispersed within the blend without thermal treatment (figure 8(a)). However in the film annealed at 250 °C, much larger PCBM clusters surrounded by the polymer nanoparticles are observed. The F8T2 layer covers the PCBM clusters, impeding electron transport to the Ca/Al electrode. It is expected that many of the photoexcitations would lead to recombination near the vicinity of the F8T2 layer.

To further support the phase separation of F8T2 and PCBM after thermal annealing, chemical analysis using XPS was employed. XPS with $Ar^+$ ions is known to damage organic samples and also cause preferential sputtering or sputter reduction. Hence, information on the chemical composition and the chemical state of the element is lost. In order to gain insights on the organic composition, the XPS with a mixture of high-energy $C_{60}^+$ ions and low-energy $Ar^+$ ions [32, 33] were used to analyze the F8T2:PCBM blends. With this co-sputtering technique, the chemical states of the organics were preserved while achieving a steady sputtering rate and increasing the probing depth. Figure 9 shows the sputter depth profile of the F8T2:PCBM blends before and after thermal annealing. Prior to thermal annealing, the chemical composition at the surface of the film (I-region) was found to be 98% C, 1% S, and 1% O (figure 9(a)). The chemical composition was significantly altered after etching for 80 minutes, indicating that the F8T2:PCBM layer was sputtered through and the indium signal increases with increasing sputter time (II-region). The uniform composition of the F8T2:PCBM layer (I-region) indicates that the PCBM is well dispersed within the F8T2 polymer matrix. The chemical analysis of the F8T2:PCBM blend annealed at 250 °C is shown in figure 9(b). In this case, the chemical composition observed can be clearly divided into three regions. The depth profile clearly shows an S rich layer (I-region) between 20 and 50 minutes, a uniformly mixed F8T2:PCBM layer (II-region) between 60 and 90 minutes, and an ITO substrate layer (III-region) after 100 minutes. The S rich layer (93% C, 6% S, 1% O) is due to the F8T2 covering the PCBM cluster, which is in good agreement with the SEM cross-section as shown in figure 8. This indicates that the thermal annealing for the F8T2:PCBM devices leads to an unfavorable phase separation,

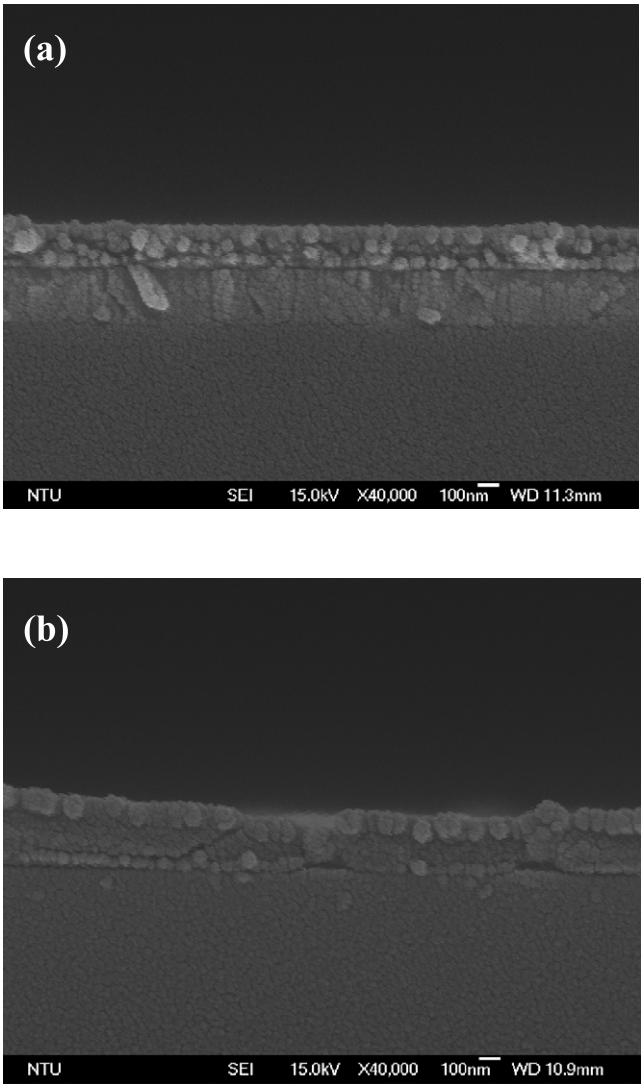


**Figure 8.** SEM side views of F8T2:PCBM blend films cast from TCB annealed at (a) 100 °C and (b) 250 °C.

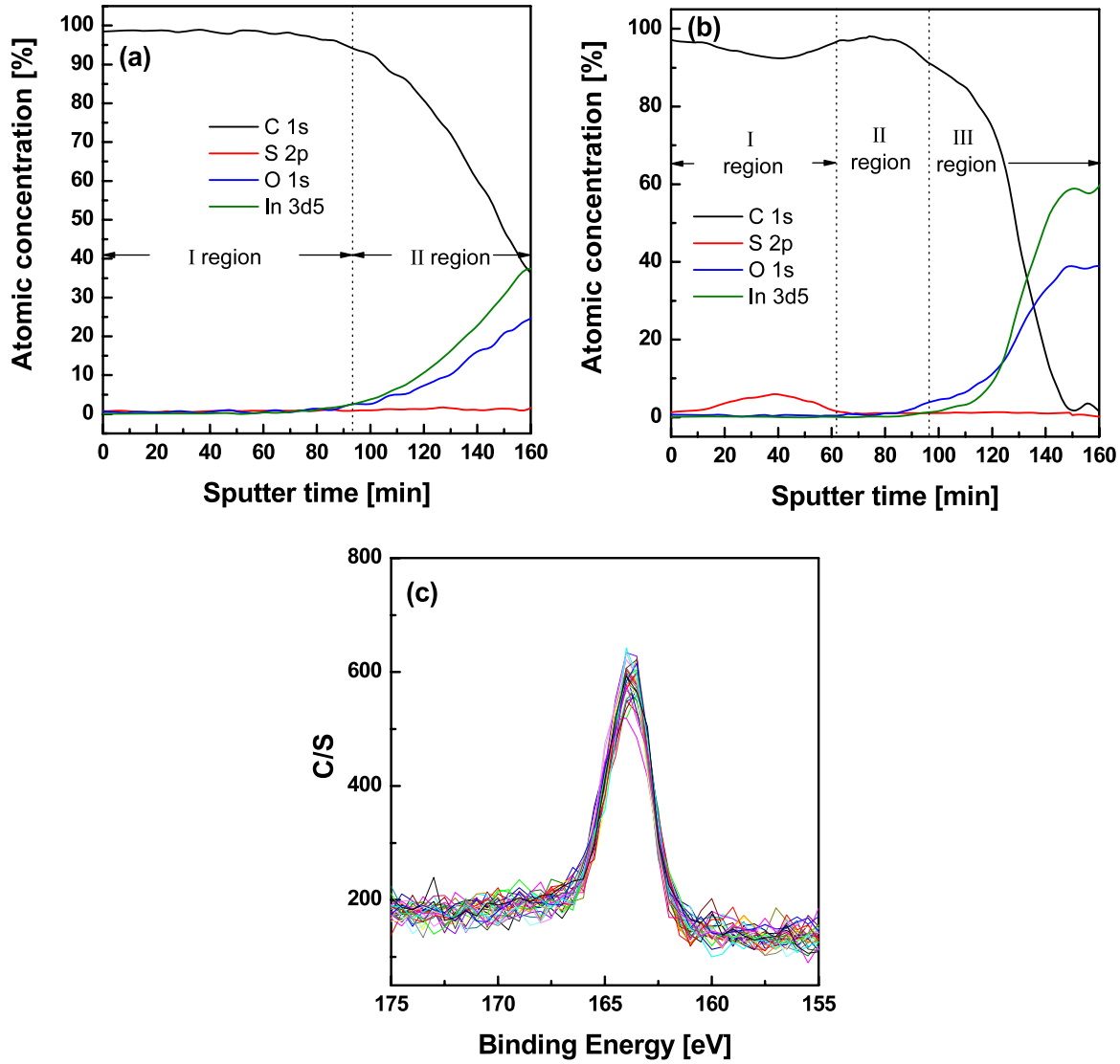


**Figure 9.** XPS depth profile of (a) F8T2:PCBM blend without thermal annealing and (b) F8T2:PCBM annealed at 250 °C using 10 kV, 10 nA $C_{60}^{+}$ mixed with a 0.2 kV, 300 Na $Ar^{+}$ beam. (c) S 2p XPS spectra of the PEDOT:PSS thin film during sputtering.

which differs greatly from the case of the P3HT:PCBM blends. Furthermore, figure 8(c) reveals the changes in S 2p XPS spectra due to ion-beam treatment. Throughout the entire sputtering process, all S 2p peaks remained at 164 eV, indicating that the chemical state is preserved. Therefore, the XPS with a mixture of high-energy $C_{60}^{+}$ ions and low-energy $Ar^{+}$ ions gun is suitable for profiling a F8T2:PCBM thin film.

To compare the effect of these different morphologies on device performance, the photovoltaic characteristics as a function of annealing temperature is shown in figure 10. The device annealed at 70 °C shows the best performance with $J_{SC}$ and PCE as high as 2.14% with an active area of 4.24 mA $cm^2$. The performance improvement after slight heating is due to the formation of F8T2 crystallites, which increases $\mu_e$ in F8T2 and achieves a more balanced charge mobility at the D/A interface. The hole and electron mobilities of the blend annealed at 70 °C are $1.12 \times 10^{-7}$ and $1.37 \times 10^{-7}$ $m^2$ $V^{-1}$ $s^{-1}$, respectively, which offer the most balanced charge transport ($\mu_e/\mu_h = 1.22$). The performance degrades with annealing temperatures higher than 70 °C. This can be rationalized by unfavorable morphologies formed via the annealing process, leading to phase separation and charge recombination as shown in figure 8. The phase separation and charge recombination lead to lower $V_{OC}$, $J_{SC}$ FF, and PCE. As a result of the influence of these two factors, it can be observed the photocurrent initially increases, but begins to decrease at an annealing temperature higher than 100 °C.

## 4. Conclusions

In conclusion, we have investigated the influence of processing conditions (blend weight ratio, solvents, and thermal annealing temperatures) on the nanomorphology of F8T2:PCBM blend films. Analysis of the changes in the film morphology suggests that the continuous carrier-conducting pathway as well as the well-balanced hole and electron transport properties can enhance device performance. These results aid understanding of the relationship between the film morphology and the

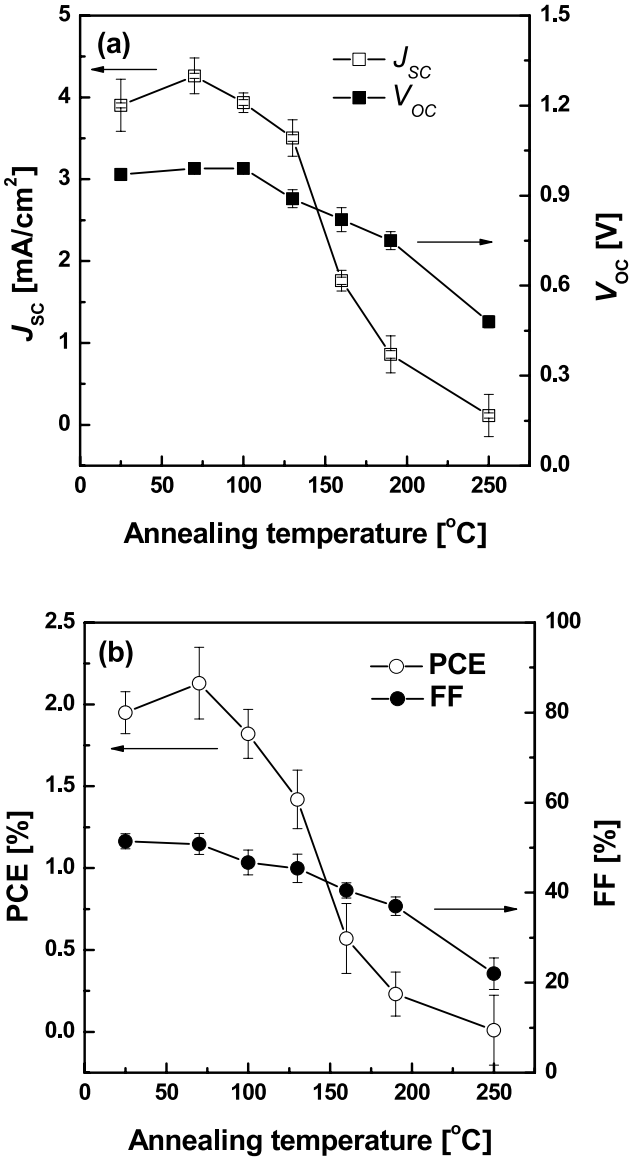


**Figure 10.** $J_{SC}$, $V_{OC}$, FF, and PCE plotted as a function of the thermal annealing temperature for the F8T2:PCBM solar cells.

device performance, and provide insights into improving the performance of polymer solar cells.

## Acknowledgments

The authors are grateful to the National Science Council (NSC), Taiwan, (NSC 97-2120-M-002-012 and 96-2221-E-001-017-MY2) and Academia Sinica, Taiwan for financial support.

## References

[1] Miller A J, Hatton R A and Silva S R P 2006 *Appl. Phys. Lett.* **89** 133117
[2] Wang M and Wang X 2008 *Sol. Energy Mater. Sol. Cells* **92** 357
[3] Tamayo A B, Walker B and Nguyen T Q 2008 *J. Phys. Chem.* C **112** 11545
[4] Pandey A K, Nunzi J M, Wang H, Oey C C, Djurišić A B, Xie M H, Leung Y H, Man K K Y and Chan W K 2007 *Org. Electron.* **8** 396
[5] Mihailetchi V D, Xie H X, de Boer B, Koster L J A and Blom P W M 2006 *Adv. Funct. Mater.* **16** 699
[6] Quiles M C, Ferenczi T, Agostinelli T, Etchegoin P G, Kim Y, Anthopoulos T D, Stavrinou P N, Bradley D D C and Nelson J 2008 *Nat. Mater.* **7** 158
[7] Dante M, Peet J and Nguyen T Q 2008 *J. Phys. Chem.* C **112** 7241
[8] Yu B Y, Tsai A, Tsai S P, Wong K T, Yang Y, Chu C W and Shyue J J 2008 *Nanotechnology* **19** 255202
[9] Lin Y Y, Chen C W, Chang J, Lin T Y, Liu I S and Su W F 2006 *Nanotechnology* **17** 1260
[10] Lin Y T, Zeng T W, Lai W Z, Chen C W, Lin Y Y, Chang Y S and Su W F 2006 *Nanotechnology* **17** 5718
[11] Blouin N, Michaud A and Leclerc M 2007 *Adv. Mater.* **19** 2295
[12] Mammo W, Admassie S, Gadisa A, Zhang F, Inganäs O and Andersson M R 2007 *Sol. Energy Mater. Sol. Cells* **91** 1010
[13] Wang E G, Wang L, Lan L F, Luo C, Zhuang W L, Peng J B and Cao Y 2008 *Appl. Phys. Lett.* **92** 033307
[14] Jespersen K G, Zhang F L, Gadisa A, Sundström V, Yartsev A and Inganäs O 2006 *Org. Electron.* **4** 235
[15] Boucle J, Ravirajan P and Nelson J 2007 *J. Mater. Chem.* **17** 3141
[16] Jo J, Vak D, Noh Y Y, Kim S S, Lim B and Kim D Y 2008 *J. Mater. Chem.* **18** 654
[17] Gather M C and Bradley D D C 2007 *Adv. Funct. Mater.* **17** 479
[18] Pattison L R, Hexemer A, Kramer E J, Krishnan S, Petroff P M and Fischer D A 2006 *Macromolecules* **39** 2225
[19] Sirringhaus H, Kawase T, Friend R H, Shimoda T, Inbasekaran M, Wu W and Woo E P 2000 *Science* **290** 2123
[20] Li S P, Newsome C J, Russell D M, Kugler T, Ishida M and Shimoda T 2005 *Appl. Phys. Lett.* **87** 062101
[21] Shrotriya V, Li G, Yao Y, Chu C W and Yang Y 2006 *Appl. Phys. Lett.* **88** 073508
[22] Shrotriya V, Yao Y, Li G and Yang Y 2006 *Appl. Phys. Lett.* **89** 063505
[23] Hoppe H, Egbe D A M, Muhlbacher D and Sariciftci N S 2004 *J. Mater. Chem.* **14** 3462
[24] Hoppe H, Niggemann M, Winder C, Kraut J, Hiesgen R, Hinsch A, Meissner D and Sariciftci N S 2004 *Adv. Funct. Mater.* **14** 1005
[25] Hoppe H and Sariciftci N S 2006 *J. Mater. Chem.* **16** 45
[26] Blom P W M, deJong M J M and vanMunster M G 1997 *Phys. Rev.* B **55** R656
[27] Dunlap D H, Parris P E and Kenkre V M 1996 *Phys. Rev. Lett.* **77** 542
[28] Gill W D 1972 *J. Appl. Phys.* **43** 5033
[29] Mihailetchi V D, van Duren J K J, Blom P W M, Hummelen J C, Janssen R A J, Kroon J M, Rispens M T, Verhees W J H and Wienk M M 2003 *Adv. Funct. Mater.* **13** 43
[30] Shrotriya V, Li G, Yao Y, Chu C W and Yang Y 2006 *Appl. Phys. Lett.* **88** 073508
[31] Li G, Shrotriya V, Yao Y, Huang J S and Yang Y 2007 *J. Mater. Chem.* **17** 3126
[32] Chen Y Y, Yu B Y, Wang W B, Hsu M F, Lin W C, Lin Y C, Jou J H and Shyue J J 2008 *Anal. Chem.* **80** 501
[33] Yu B Y, Chen Y Y, Wang W B, Hsu M F, Tsai S P, Lin W C, Lin Y C, Jou J H, Chu C W and Shyue J J 2008 *Anal. Chem.* **80** 3412